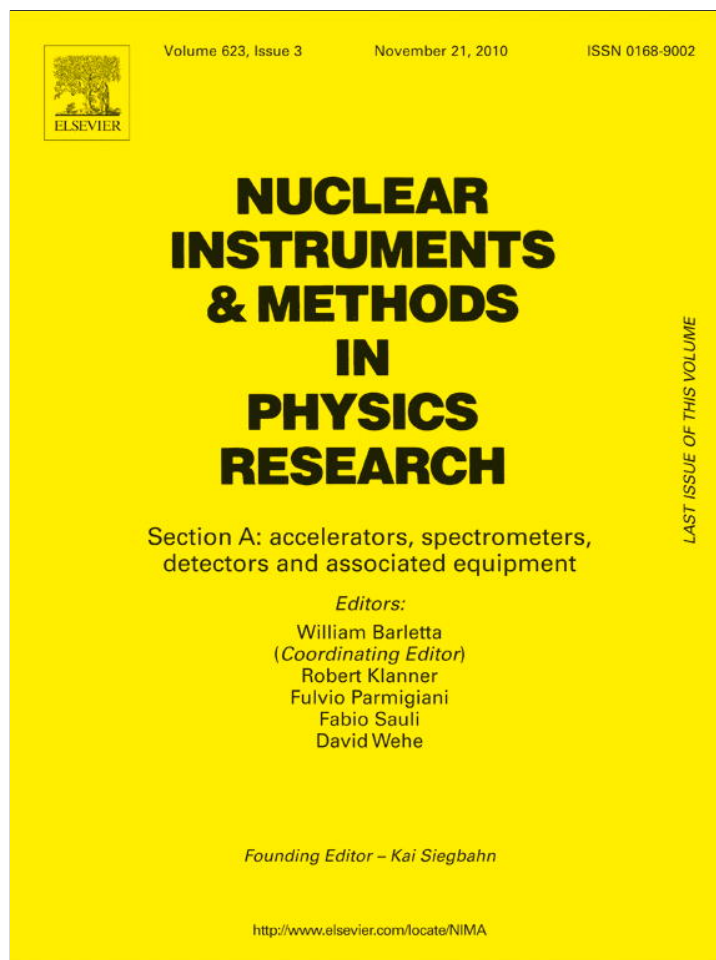


Provided for non-commercial research and education use.
Not for reproduction, distribution or commercial use.



This article appeared in a journal published by Elsevier. The attached copy is furnished to the author for internal non-commercial research and education use, including for instruction at the authors institution and sharing with colleagues.

Other uses, including reproduction and distribution, or selling or licensing copies, or posting to personal, institutional or third party websites are prohibited.

In most cases authors are permitted to post their version of the article (e.g. in Word or Tex form) to their personal website or institutional repository. Authors requiring further information regarding Elsevier's archiving and manuscript policies are encouraged to visit:

<http://www.elsevier.com/copyright>



Contents lists available at ScienceDirect

Nuclear Instruments and Methods in Physics Research A

journal homepage: www.elsevier.com/locate/nima

Studies on the efficiency of the neutron shielding for the SIMPLE dark matter search

A.C. Fernandes^{a,b,*}, M. Felizardo^{c,a}, A. Kling^{a,b}, J.G. Marques^{a,b}, T. Morlat^b^a Instituto Tecnológico e Nuclear, Unidade de Reactores e Segurança Nuclear, Estrada Nacional 10, 2686-953 Sacavém, Portugal^b Centro de Física Nuclear da Universidade de Lisboa, Av. Prof. Gama Pinto, 2, 1649-003 Lisboa, Portugal^c Departamento de Física, Faculdade de Ciências e Tecnologia, Universidade Nova de Lisboa, 2829-516 Caparica, Portugal

ARTICLE INFO

Article history:

Received 26 April 2010

Received in revised form

30 June 2010

Accepted 12 July 2010

Available online 16 July 2010

Keywords:

Dark matter

Underground laboratory

Neutron background

MCNP simulation

ABSTRACT

The SIMPLE project for direct dark matter search is located in a deep underground laboratory, where non-WIMP signals are expected due to neutrons and alpha particles naturally occurring in the facility. This work presents a first study on the efficiency of the neutron shielding for SIMPLE and possible routes for its optimization. The evaluation of the neutron component considers spontaneous fission and (α,n) neutrons originating from the ^{238}U and ^{232}Th present in the experiment materials. Using recently published data on (α,n) yields and spectra, a Monte Carlo model using the MCNP code is employed to simulate the transport of both spontaneous fission and (α,n) neutrons. The application of MCNP offers an alternative method to the SOURCES code used systematically by others for the evaluation of the (α,n) component. Results supporting the optimization of the neutron shield for SIMPLE are described and the feasibility of reducing the event rate to less than 1 evt/kgd is demonstrated.

© 2010 Elsevier B.V. All rights reserved.

1. Introduction

Dark matter search experiments are designed to detect astroparticle dark matter candidates, generically called Weakly Interacting Massive Particles (WIMPs). For direct WIMP detection, less than 1 event per day is expected to occur in 1 kg of detector mass (1 evt/kgd). Although search experiments are performed in deep underground facilities, where the rock overburden shields against the cosmic rays, discrimination of these phenomena against more frequently occurring background signals from the natural radioactivity of the underground site and detector materials requires additional methods for background suppression or rejection.

Superheated Instrument for Massive Particle Experiments (SIMPLE), located at the LSBB (Laboratoire Souterrain à Bas Bruit, Pays d'Apt, southern France) underground laboratory [1], is one of many experiments to search for evidence of WIMP interactions. Fluorine-loaded Superheated Droplet Detectors (SDDs) are used, as their intrinsic insensitivity to low Linear Energy Transfer ($\text{LET} < 150 \text{ keV } \mu\text{m}^{-1}$) particles eliminates a significant part of the potential background events, such as muons, electrons and photons. A general description of the SIMPLE experiment and

the latest measurement results can be found in Refs. [2,3], respectively.

Due to the LET detection threshold the main contributions to the background signal of SIMPLE stem from alpha particles (due to environmental radon and radio-impurities in the detector material) and neutrons with energies larger than 8 keV. These are produced in (i) spontaneous fission, mostly from the ^{238}U present in the materials that surround and constitute the detectors; (ii) (α,n) interactions due to natural alpha-emitters such as uranium and thorium; (iii) nuclear reactions induced by cosmic muons. As the latter contribution decreases exponentially with increase in facility depth, it is relatively small in deep underground sites, where the background neutron field is essentially due to the occurrence of U and Th in the materials. Monte Carlo calculations of the neutron background in such experiments have been performed by various authors [4–6]. A review of the various methods used is given in Ref. [7]. General-purpose codes like FLUKA, GEANT and LAHET are applied to simulate the production of muon-induced neutrons, for neutron transport and source propagation (MCNP and MCNPX are also applied for the two latter purposes). The production of (α,n) neutrons is generally dealt with using SOURCES, a code specifically developed for the determination of neutron production rates and spectra from (α,n) reactions, spontaneous fission and delayed neutron emission due to the decay of various radionuclides. SOURCES is often modified in order to extend the upper energy range of the alpha particles under consideration from 6.5 MeV in the original version. Recently published data of energy spectra

* Corresponding author at: Instituto Tecnológico e Nuclear, Unidade de Reactores e Segurança Nuclear, Estrada Nacional 10, 2686-953 Sacavém, Portugal. Tel.: +351 219946152; fax: +351 219941039.

E-mail address: anafer@itn.pt (A.C. Fernandes).

and production yields of (α ,n) neutrons in materials containing ^{238}U , ^{232}Th or ^{nat}Sm [8] offer an alternative to SOURCES and can be incorporated directly in the source term of the general-purpose codes.

In this work the efficiency of the SIMPLE shielding against the neutron contribution (from spontaneous fission and (α ,n) reactions) to the background signal of the SIMPLE experiment is evaluated using the MCNP code (version 5) [9]. The results suggest the necessity of additional neutron shielding for the SDDs, which are similarly evaluated in order to obtain event rates smaller than 1 evt/kgd.

2. Geometry and materials

Each SSD consists of a 900 ml glycerin-based gel matrix with a 12–20 g suspension of superheated R-115 liquid (C_2ClF_5), contained in a square glass flask of 12 cm height. The current SIMPLE experiment uses fifteen detectors installed in a water bath inside a $97 \times 130 \times 65 \text{ cm}^3$ tank. The SDDs are distributed in alternating positions in a 16 cm square lattice and can be raised as much as 50 cm above the tank floor. A water layer of 3 cm above the glycerin level limits the diffusion of atmospheric radon into the detectors; the use of high radiopurity food materials provides an α -contamination level smaller than 0.5 evt/kgd.

The tank is located within a 60 m^3 room at a depth of 1500 mwe (meter water equivalent) within the LSBB. The surrounding rock is calcite. Floor plan dimensions are $400 \times 564 \text{ cm}^2$. The room is equipped with a 1 cm-thick steel lining forming a Faraday cage. The ceiling has a semi-cylindrical shape (diameter 404 cm), the room height varying between 212 and 305 cm. Room walls, ceiling and floor consist of concrete, with a thickness between 30 and 100 cm. The room floor contains several steel-covered, 50 cm deep crawl spaces previously used for cable conduits. The tank sits on a wooden support structure with a 32 cm height above the concrete floor in the central region of the room (the latter is further referred to as the “tank pedestal”).

The current shielding of the experiment consists of 50 cm water in the tank, below the SDDs, and a “castle” of 20 l water boxes $22 \times 25 \times 38 \text{ cm}^3$ symmetrically installed around and above the tank to produce water thicknesses of 50 and 75 cm, respectively. The tank pedestal is surrounded by an arrangement of water boxes (height $50 \times$ width 50) cm. Some water boxes are slightly deformed due to the weight loading, leading to gaps in the lateral part of the shield.

Fig. 1 presents a schematic view of the room, assuming a uniform concrete thickness. Some structures are removed from the figure for clarity (rock, left concrete wall, front water shield and tank water above and around the detectors). The water shield pieces placed along the room length (left and right in the figure) will be designated as “side shield”, while those facing the room ends (not represented in the figure) will be referred to as “end shield”.

MCNP input requires a description of the facility geometry and materials (elemental composition and density) where neutron transport is simulated. Unless explicitly mentioned, constant concrete and rock thicknesses of 30 cm and 1 m, respectively, were used in the simulations. The ENDF-B6.0 neutron cross-section library, included in the MCNP package, was used to describe neutron interactions with the materials.

The neutron source is defined in terms of energy spectrum and location. As MCNP outputs are given relative to one source neutron, a final scaling to the actual source emission rate is performed in order to obtain absolute results.

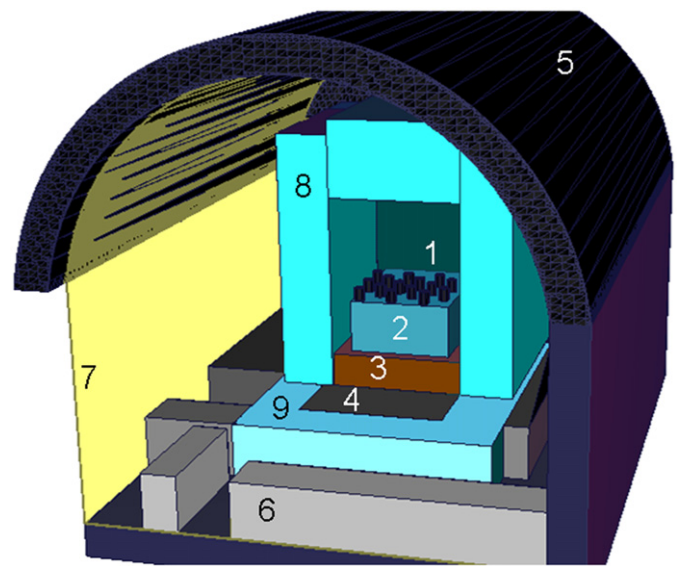


Fig. 1. Schematic view of the room and experimental set-up. 1: Detectors; 2: tank (water below the detectors); 3: wood support; 4: tank pedestal; 5: room ceiling, walls and floor; 6: concrete floor structures defining the cable conduits; 7: steel lining; 8: water shield around and above the detectors; 9: water shield around the tank pedestal.

Table 1
Measured composition of rock and concrete (in weight %).

| | Concrete | Rock |
|-------------------------|----------|-------|
| SiO_2 | 37.20 | – |
| Al_2O_3 | 3.58 | – |
| Fe_2O_3 | 1.40 | – |
| MnO | 0.05 | – |
| MgO | 0.75 | 0.31 |
| CaCO_3 | 55.42 | 99.69 |
| Na_2O | 0.67 | – |
| K_2O | 0.72 | – |
| TiO_2 | 0.15 | – |
| P_2O_5 | 0.06 | – |

Chemical analyses of rock and concrete yielded the compositions described in Table 1. Various trace metals present at the ppm level were not considered in the materials description. The analyses indicated that the amount of U in the rock is approximately half of that in concrete. Th was not identified. Values measured for other underground laboratories in continental Europe (CanFranc, Gran Sasso, Modane) [10–12] range from 2 to 70 ppb. As an estimate the average value obtained for these sites (40 ppb) is used in this work.

The composition and density of steel were assumed to be those of iron (density 7.874 g cm^{-3}). Standard compositions and densities for air (volume composition 78% N_2 +21% O_2 +1% Ar, density $1 \times 10^{-3} \text{ g cm}^{-3}$), water (H_2O , density 1 g cm^{-3}) and glycerin ($\text{C}_3\text{H}_5(\text{OH})_3$, density 1.261 g cm^{-3}) were used. The measured density of rock is $2.61 \pm 0.01 \text{ g cm}^{-3}$. For concrete, a density of 3 g cm^{-3} was assumed (standard densities for ordinary Portland and heavy weight baryte concrete are 2.3 and 3.4 g cm^{-3} , respectively [13]).

In order to define the neutron source, the ^{238}U and ^{232}Th amounts for the various materials were measured or estimated (Table 2).

Samples of concrete and steel were analyzed by gamma spectrometry in order to quantify the amount of neutron emitters. From the evaluation of concrete, the detection of ^{238}Ac and ^{234m}Pa

Table 2

Activity concentration of neutron emitters in materials (see Section 6 for a discussion on uncertainties). When necessary, conversion between activity and mass has been made using the following factors: 1 Bq=80.27 $\mu\text{g}({}^{238}\text{U})$ and 1 Bq=245.40 $\mu\text{g}({}^{232}\text{Th})$.

| | ${}^{238}\text{U}$ (Bq kg ⁻¹) | ${}^{232}\text{Th}$ (Bq kg ⁻¹) |
|----------|---|--|
| Concrete | 10.5 ± 1 | 7.7 ± 0.2 |
| Steel | 3.6 × 10 ⁻² | 1.3 × 10 ⁻² |
| Rock | 5.0 ± 2.5 | (1.6 ± 1.3) × 10 ⁻¹ |
| Water | 5.0 ± 3.0 × 10 ⁻³ | 1.0 × 10 ⁻² |

allowed to derive the activity concentrations of ${}^{238}\text{U}$ and ${}^{232}\text{Th}$, respectively. The analysis of steel results is very complex because the equilibrium of the natural decay chains of ${}^{238}\text{U}$ and ${}^{232}\text{Th}$ has been distorted by the steel smelting (see Section 6.3). From the available information (${}^{234}\text{Th}$, ${}^{226}\text{Ra}$ and ${}^{210}\text{Pb}$ as ${}^{238}\text{U}$ -related decay products and ${}^{228}\text{Ra}$ and ${}^{228}\text{Th}$ for ${}^{232}\text{Th}$) it was deduced that the activity of ${}^{232}\text{Th}$ is equal to that of its chemically identical decay isotope ${}^{228}\text{Th}$, while ${}^{238}\text{U}$ activity is equal to that of ${}^{234}\text{Th}$ —a direct descendent with a half life of 24 d, which is much smaller than the steel age (LSBB was built in the late seventies).

The ${}^{238}\text{U}$ content in the shield water was estimated as 5 mBq l⁻¹, on the basis of data provided by IRSN (French Institute for Radioprotection and Nuclear Safety) concerning the neighboring region of Cadarache (2–7 mBq l⁻¹) [14]. Since no values for Th are available, an activity concentration of 10 mBq ${}^{232}\text{Th}$ l⁻¹ was assumed considering values measured in other European countries [15,16].

3. Neutron source

The source term includes isotropically emitted spontaneous fission and (α ,n) neutrons due to the presence of U and Th in the concrete, steel lining, shield water and rock. Internal contamination from the SDDs is not accounted for, because the devices are produced using purified materials [2].

The probability that the decay occurs via spontaneous fission is $1.80 \times 10^{-9}\%$ (${}^{232}\text{Th}$) and $5.45 \times 10^{-5}\%$ (${}^{238}\text{U}$). In a spontaneous fission, 2.14 (${}^{232}\text{Th}$) and 2.01 (${}^{238}\text{U}$) neutrons are produced in average [17]. Their energy distribution is commonly described by the Watt formula using the default MCNP parameters. As the amount of Th and U in the materials is of the same order of magnitude, most spontaneous fission-produced neutrons are due to ${}^{238}\text{U}$.

Unlike spontaneous fission, neutrons from (α ,n) interactions have material-dependent energy distributions. Neutron spectra in the energy interval of 100 keV–15 MeV were obtained from Ref. [8], and are represented in Fig. 2.

Table 3 contains the neutron source yield per microgram of neutron emitter and year, together with the average and most probable energies of the emitted neutrons. With the exception of iron, the average energy of (α ,n) neutrons is higher than that of spontaneous fission neutrons. A higher penetration probability of (α ,n) neutrons through the shield is expected, which may partly compensate the smaller emission yield.

4. Calculation of event rates

MCNP output is accompanied by a statistical uncertainty that decreases with the number of neutrons detected in a target volume. For uncertainty/computation time reduction, the set of SDDs was replaced by a single 12 cm-thick glycerin layer that extends over the whole tank cross-sectional area (Fig. 3).

For a detection efficiency of 100% [2], each neutron that enters the detector volume will produce one event. An F1 tally (surface current) with angular bins of 0°, 90° and 180° perpendicular to each detector surface was used to count all neutrons that enter its volume. An F4 tally (track length estimator) was used to calculate the average neutron fluence rate (ϕ) in the detector volume.

A lower energy cut-off of 1 keV was used to reduce the computation time spent with the simulation of neutrons that do not contribute to the detector signal. Only neutrons with energy larger than the SDDs detection threshold of 8 keV were tallied. The computing time for one million particles was 1–3 min in a Core-2-Duo, 2.80 GHz personal computer.

As the detector volume considered in the simulations is different from the actual, the output is further scaled to the actual volume and active mass. The calculated event rate is multiplied by the real-to-model detection volume ratio and divided by the active mass contained in the fifteen SDDs (208.7 g).

For the optimization of the neutron shield, various configurations were evaluated, considering only neutrons emitted from concrete and water. The wooden support was not included in the models and the tank effectively floated above the pedestal. Various materials may be interposed in the gap between the pedestal and the tank for future shielding improvements.

- Configuration #1*: In the initial model, the shield consisted only of rock and concrete to protect against the cosmic radiation. The SDDs were placed in the tank with 14 cm water below; 9 cm water covered the detectors.
- Configuration #2*: A 50 cm water shield was installed around the tank to reduce the event rate.
- Configuration #3*: The detectors were raised within the tank to establish a 50 cm water layer below (the maximum achievable). In addition, water was placed around the tank pedestal to shield against the floor. The water shield above the tank was enlarged to 75 cm water for protection from eventual muon-induced neutrons produced in the rock.

5. Results

5.1. Shield evaluation

Table 4 shows the calculated event and neutron fluence rates, considering the different neutron emission processes within concrete and water. The relative contributions of the various concrete regions to the overall event rate were discriminated (Table 5) in order to orient the shield optimization process.

- Configuration #1*: The calculated event rate was 1047 evt/kgd, mostly from concrete, with similar contributions from spontaneous fission (α ,n) from ${}^{238}\text{U}$ and (α ,n) from ${}^{232}\text{Th}$.
- Configuration #2*: With 50 cm water around and above the tank, neutrons from the room walls and ceiling were attenuated by a factor of $2\text{--}4 \times 10^4$. A significant contribution of neutrons from the floor and especially the tank pedestal persisted, yielding 38 evt/kgd. The contribution due to the water remained negligible in comparison to the total event rate.
- Configuration #3*: Calculations yielded the value of 6 evt/kgd, mainly due to the tank pedestal.

5.2. Event rates

The event rate was calculated for Configuration #3, which was implemented in recent SIMPLE experiments. The calculation

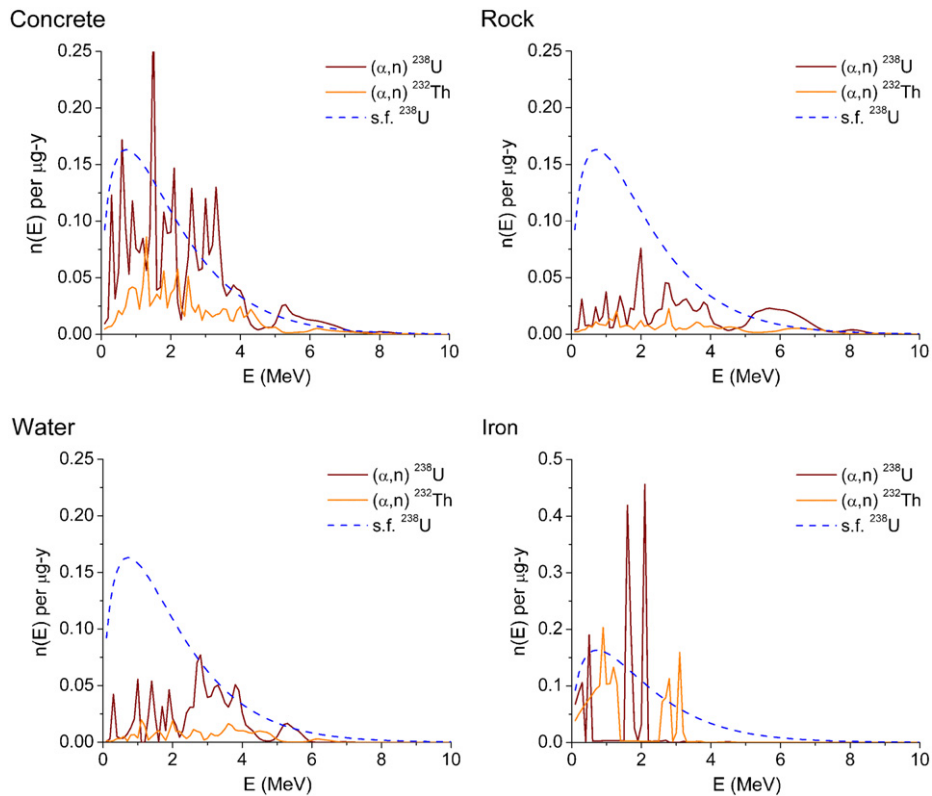


Fig. 2. Spectra of decay-induced (α,n) neutrons due to the presence of ^{238}U and ^{232}Th in various materials [8]. The Watt distribution representing spontaneous fission (s.f.) neutrons is also represented.

Table 3
Neutron source data.

| Production reaction | Yield ($\mu\text{g}^{-1}\text{y}^{-1}$) | Average energy (MeV) | Most probable energy (MeV) |
|---|---|----------------------|----------------------------|
| Spontaneous fission of ^{238}U | 0.449 | 2.0 | 0.7 |
| (α,n) from ^{238}U in rock | 0.137 | 3.5 | 2.0 |
| (α,n) from ^{232}Th in rock | 0.0458 | 3.3 | 2.8 |
| (α,n) from ^{238}U in concrete | 0.344 | 2.4 | 1.5 |
| (α,n) from ^{232}Th in concrete | 0.128 | 2.5 | 1.3 |
| (α,n) from ^{238}U in water | 0.129 | 2.8 | 2.8 |
| (α,n) from ^{232}Th in water | 0.0403 | 3.0 | 1.1 |
| (α,n) from ^{238}U in iron | 0.165 | 1.4 | 2.1 |
| (α,n) from ^{232}Th in iron | 0.173 | 1.4 | 0.9 |

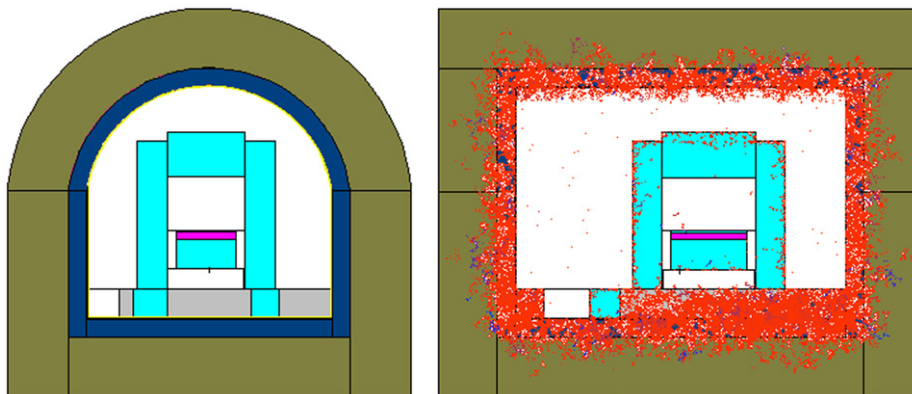


Fig. 3. Model used in the MCNP simulations. Left: vertical front view; right: vertical sideview, with the representation of interactions of neutrons emitted from concrete.

includes the contributions from spontaneous fission and (α ,n) neutrons originating from water, concrete, steel and rock. In the case of rock, all source neutrons were created in a depth interval of 30 cm starting at the concrete–rock interface.

The results presented in Table 6 indicate that the steel lining and the rock contribute negligibly to the SDD signal. In the case of steel, this is due to the small amount of material, the reduced content of ^{238}U and ^{232}Th and the low energy of the (α ,n) neutrons. The small contribution of rock can be explained by the neutron attenuation due to the concrete. As will be discussed in Section 6.1, neutrons from concrete layers at a depth larger than 20 cm are attenuated by the shallower regions, yielding an event rate that is independent of the concrete thickness. The same applies to the neutrons from the rock, which are strongly attenuated by the 30 cm concrete layer, especially as the amount of U in the rock is smaller than in concrete. This justifies the application of the source configuration mentioned

Table 4
Calculated event rates for different shielding configurations. Statistical uncertainties are smaller than 2%.

| Neutron origin | Event rate (evt/kgd) (%) | | |
|---------------------------------------|--------------------------|----------------------|----------------------|
| | Configuration #1 | Configuration #2 | Configuration #3 |
| <i>Concrete</i> | | | |
| Spont. fission | 329 | 14 | 2.5 |
| (α ,n) from ^{238}U | 356 | 13 | 2.1 |
| (α ,n) from ^{232}Th | 362 | 11 | 1.8 |
| <i>Subtotal</i> | 1047 | 38 | 6.4 |
| <i>Water</i> | | | |
| Spont. fission | 1.4×10^{-2} | 2.0×10^{-2} | 2.1×10^{-2} |
| (α ,n) from ^{238}U | 5.0×10^{-7} | 7.5×10^{-7} | 7.8×10^{-7} |
| (α ,n) from ^{232}Th | 3.5×10^{-5} | 1.5×10^{-2} | 1.5×10^{-2} |
| <i>Subtotal</i> | 1.8×10^{-2} | 3.5×10^{-2} | 3.6×10^{-2} |

Table 5
Relative contributions of the various concrete regions to the event rate produced by spontaneous fission neutrons in concrete.

| Concrete region | Event rate (evt/kgd) (%) | | |
|-----------------|--------------------------|------------------|------------------|
| | Configuration #1 | Configuration #2 | Configuration #3 |
| End walls | 20 | 0.2 | 0.3 |
| Side walls | 23 | 0.6 | <0.3 |
| Ceiling | 28 | 0.2 | <0.2 |
| Floor | 29 | 99 | 99 |

Table 6
Calculated neutron fluence and event rates from the various materials and reactions. The source volume and number of particle stories (nps) simulated are indicated.

| Material | Volume (m ³) | nps | Reaction | ϕ (cm ⁻² s ⁻¹) (%) | Event rate (evt/kgd) (%) |
|------------------|--------------------------|-------|---------------------------------------|--|-------------------------------|
| Concrete (30 cm) | 42.671 | 50 M | Spont. fission | $1.60 \times 10^{-9} \pm 3$ | 2.51 ± 2 |
| | | | (α ,n) from ^{238}U | $1.42 \times 10^{-9} \pm 3$ | 2.11 ± 2 |
| | | | (α ,n) from ^{232}Th | $1.25 \times 10^{-9} \pm 3$ | 1.78 ± 2 |
| | | | <i>Subtotal</i> | $4.27 \times 10^{-9} \pm 2$ | 6.40 ± 1 |
| Water | 13.451 | 5 M | Spont. fission | $2.69 \times 10^{-11} \pm 1$ | $2.12 \times 10^{-2} \pm 1$ |
| | | | (α ,n) from ^{238}U | $1.10 \times 10^{-15} \pm 1$ | $7.75 \times 10^{-6} \pm 0.5$ |
| | | | (α ,n) from ^{232}Th | $2.18 \times 10^{-11} \pm 1$ | $1.51 \times 10^{-2} \pm 0.5$ |
| | | | <i>Subtotal</i> | $4.87 \times 10^{-11} \pm 0.7$ | $4.40 \times 10^{-2} \pm 0.5$ |
| Steel | 1.072 | 1 G | Spont. fission | $3.98 \times 10^{-14} \pm 3$ | $3.75 \times 10^{-5} \pm 2$ |
| | | | (α ,n) from ^{238}U | $2.11 \times 10^{-15} \pm 13$ | $4.87 \times 10^{-6} \pm 9$ |
| | | | (α ,n) from ^{232}Th | $4.60 \times 10^{-15} \pm 5$ | $7.52 \times 10^{-6} \pm 3$ |
| | | | <i>Subtotal</i> | $4.65 \times 10^{-14} \pm 3$ | $4.99 \times 10^{-5} \pm 2$ |
| Rock (30 cm) | 46.751 | 500 M | Spont. fission | $1.53 \times 10^{-12} \pm 22$ | $1.44 \times 10^{-3} \pm 16$ |
| | | | (α ,n) from ^{238}U | $5.88 \times 10^{-13} \pm 21$ | $5.42 \times 10^{-4} \pm 17$ |
| | | | (α ,n) from ^{232}Th | $1.28 \times 10^{-14} \pm 23$ | $1.36 \times 10^{-5} \pm 18$ |
| | | | <i>Subtotal</i> | $2.13 \times 10^{-12} \pm 17$ | $2.00 \times 10^{-3} \pm 12$ |
| Total | | | | $4.32 \times 10^{-9} \pm 2.0$ | 6.45 ± 0.99 |

above, thereby improving the statistical uncertainty without modifying the calculated result.

6. Uncertainty analysis

Non-statistical uncertainties are those that actually limit the result precision, since the statistical uncertainties can be made negligible by increasing the number of source particles simulated or any of the variance reduction techniques available in MCNP. The origin of various non-statistical uncertainties is discussed as follows.

6.1. Concrete thickness

The impact of the varying concrete thickness on the calculated event rates was evaluated via simulations that considered different concrete thicknesses. Table 7 shows that the event rate is independent of this parameter for thicknesses larger than 20 cm.

6.2. Concrete density

As U and Th contents in concrete are given in weight fractions, an increased concrete density relative to the assumed value is immediately associated with a higher neutron source emission rate. On the other hand, neutron attenuation is stronger with higher density concrete. The event rates were calculated for concrete densities varying 15% relative to the assumed value of 3 g cm^{-3} . The results presented in Table 8 show a small increase in the event rate with the concrete density, yielding a maximum variation of 2.9% with respect to the reference value.

6.3. Neutron emitters

a) *Emitters in water:* The SDDs are directly exposed to the radiation emitted by the water shield. Therefore, a radio-assay of the water is essential in the future to clarify its actual contribution to the signal and reduce the calculation uncertainty. The results from Table 6 show that the water contribution to the SDD signal is very small for the assumed activity concentrations. An uncertainty of 60% is estimated for the ^{238}U content in water, based on the variation limits of the IRSN monitoring measurements. For ^{232}Th similar information is not available, which impedes the estimate of a reliable uncertainty.

Table 7

Calculated event rates from concrete with different thicknesses.

| Concrete thickness (cm) | Event rate (evt/kgd) (%) | | | |
|-------------------------|--------------------------|--------------------------------------|---------------------------------------|--------------|
| | Spont. fission | (α,n) from ^{238}U | (α,n) from ^{232}Th | Total |
| 10 | 2.39 \pm 3 | 1.99 \pm 2 | 1.66 \pm 2 | 6.04 \pm 1 |
| 20 | 2.50 \pm 3 | 2.12 \pm 3 | 1.78 \pm 2 | 6.40 \pm 1 |
| 30 | 2.51 \pm 2 | 2.11 \pm 2 | 1.78 \pm 2 | 6.40 \pm 1 |
| 50 | 2.55 \pm 2 | 2.05 \pm 3 | 1.80 \pm 3 | 6.40 \pm 2 |
| 70 | 2.50 \pm 4 | 2.13 \pm 3 | 1.84 \pm 3 | 6.47 \pm 2 |
| 100 | 2.50 \pm 2 | 2.10 \pm 2 | 1.74 \pm 2 | 6.34 \pm 1 |
| Average (30–100 cm) | 2.52 \pm 1 | 2.10 \pm 1 | 1.79 \pm 1 | 6.40 \pm 1 |

Table 8

Calculated event rates from concrete with different densities.

| Concrete density (g cm^{-3}) | Event rate (evt/kgd) (%) | | | |
|---|--------------------------|--------------------------------------|---------------------------------------|--------------|
| | Spont. fission | (α,n) from ^{238}U | (α,n) from ^{232}Th | Total |
| 2.60 | 2.44 \pm 2 | 2.05 \pm 2 | 1.73 \pm 2 | 6.22 \pm 1 |
| 3.00 | 2.51 \pm 3 | 2.11 \pm 3 | 1.78 \pm 2 | 6.40 \pm 2 |
| 3.45 | 2.54 \pm 2 | 2.20 \pm 2 | 1.75 \pm 2 | 6.49 \pm 1 |

Table 9

Relative contribution to the neutron fluence rate in the detector volume due to neutrons that pass through a gap in the water shield. Only spontaneous-fission neutrons from concrete are considered.

| Gap size (mm) | ϕ (%) | | |
|---------------|------------------------|-------------------------|-----------------|
| | Gaps in the end shield | Gaps in the side shield | Total (28 gaps) |
| 1 | 0.081 \pm 0.005 | 0.065 \pm 0.005 | 2.0 \pm 0.1 |
| 3 | 0.118 \pm 0.007 | 0.096 \pm 0.006 | 3.0 \pm 0.1 |
| 6 | 0.24 \pm 0.01 | 0.199 \pm 0.009 | 6.2 \pm 0.2 |
| 10 | 0.49 \pm 0.01 | 0.42 \pm 0.02 | 12.8 \pm 0.3 |
| 13 | 0.77 \pm 0.02 | 0.68 \pm 0.02 | 20.4 \pm 0.4 |
| 16 | 1.15 \pm 0.03 | 1.00 \pm 0.03 | 29.6 \pm 0.6 |
| 20 | 1.67 \pm 0.04 | 1.51 \pm 0.04 | 44.4 \pm 0.8 |

- b) *Emitters in steel*: The absence of secular equilibrium of the ^{238}U and ^{232}Th in steel is demonstrated by the distinct measured activity concentrations for ^{234}Th , ^{226}Ra and ^{210}Pb (36 ± 11 , 10 ± 1 and 1740 ± 200 mBq kg^{-1} , respectively) as ^{238}U -related decay products and ^{228}Ra and ^{228}Th (6 ± 2 and 3 ± 1 mBq kg^{-1} , respectively) for ^{232}Th . Since the estimates on ^{238}U and ^{232}Th contents in steel were based solely on one of their respective decay products (although chosen by sound reasoning) uncertainties are omitted.
- c) *Emitters in rock*: From the results of Table 6, the presence of neutron emitters in rock has a negligible effect, unless their content is significantly higher than in concrete (^{238}U or ^{232}Th activity concentrations in the order of 10^3 or 10^4 Bq kg^{-1} would be required to produce 1 evt/kgd, respectively). Although a radio-assay of the rock can be useful to verify this assumption, no serious consequences are expected. As mentioned in Section 2, the U content is determined via chemical analysis. Based on the discrepancies observed between the chemical and radio-assays in the case of concrete (1.21 and 0.85 ppm, respectively) an uncertainty of 50% with respect to the ^{238}U content in rock appears to be reasonable. Regarding ^{232}Th an uncertainty of 80% is suggested to cover the range of values reported for the underground laboratories mentioned above.
- d) *Emitters in concrete*: Radio-assay of the concrete determined the ^{238}U and ^{232}Th contents with uncertainties at the one-sigma level (67% level of confidence) of 10% and 3%,

respectively. Since ^{238}U in concrete represents approximately two-thirds of the SDDs event rate, this will be a major component of the uncertainty.

6.4. Effect of gaps in the water shield

The influence that gaps in the water shield may have on the detector signal was estimated. Simulations including gaps that extend over the whole shield height were performed for gap widths up to 20 mm in the end and side shields. Neutrons passing through the gaps were identified using the cell flagging option in the F4 tally. Table 9 shows the contribution of one gap to the detector signal. Considering seven 1 cm-wide gaps in each shield face (a worst-case scenario), the event rate is increased by 13% relative to a perfect shield. This value is included in the uncertainty of the calculated detector signal.

6.5. Muon-induced neutrons

The interaction of cosmic-ray muons with rock generates neutrons with average energies on the order of 80 ± 20 MeV that emerge from the cavern surface and contribute to the detector signal. The angular distribution of the emitted neutrons is quite complex: spallation-produced neutrons are preferentially emitted in the muon direction, while the secondary evaporation of neutrons is predominantly isotropic.

Table 10

Combined statistical and non-statistical uncertainties (two significant digits) in the calculated event rate. Statistical and non-statistical uncertainties are indicated as types A and B, respectively.

| Uncertainty Id. | Quantity | Uncertainty in quantity | Type | Origin of uncertainty | Sensitivity coefficient (%) | Relative uncertainty (%) |
|-----------------------------------|-----------------------|-------------------------|------|---|-----------------------------|--------------------------|
| Statistical | Event rate | 0.99% | A | Simulation | 100 | 0.99 |
| 6.1 | Concrete thickness | 30–100 cm | B | Variation limits | 0.00 | 0.00 |
| 6.2 | Concrete density | 15% | B | Standard concrete densities | 20 | 3.0 |
| 6.3 a | U in water | 60% | B | Reference levels in neighboring regions | 0.33 | 0.20 |
| | Th in water | 100% | B | | 0.23 | 0.23 |
| 6.3 b | U in steel | 100% | B | Non-equilibrium of steel | 7.5×10^{-5} | 7.5×10^{-5} |
| | Th in steel | 100% | B | | 1.2×10^{-4} | 1.2×10^{-4} |
| 6.3 c | U in rock | 50% | B | Chemical analysis | 3.0×10^{-2} | 1.5×10^{-2} |
| | Th in rock | 80% | B | | 2.1×10^{-4} | 1.7×10^{-4} |
| 6.3 d | U in concrete | 10% | B | Measurement uncertainty | 72 | 7.2 |
| | Th in concrete | 3% | B | | 28 | 0.83 |
| 6.4 | Gaps in water shield | 100% | B | Calculated contribution | 13 | 13 |
| 6.5 | Muon-induced neutrons | 100% | B | Estimated contribution | 0.46 | 0.46 |
| Combined relative uncertainty (%) | | | | | | 15 |

MCNP presents serious limitations concerning the simulation of muon-induced neutrons, as muon transport is not implemented in the code and standard neutron interaction cross-section libraries are limited to 20 MeV. In this work, a rough estimate of the signal produced by muon-induced neutrons was made based on a detailed investigation of the muon-induced background in several other underground laboratories [18]. According to this study, the neutron fluence rate at 1500 mwe is $4 \times 10^{-8} \text{ cm}^{-2} \text{ s}^{-1}$ and its energy distribution is approximately described by the following probability numbers: 75% ($< 1 \text{ MeV}$); 5% ($1\text{--}10 \text{ MeV}$); 20% ($10\text{--}100 \text{ MeV}$) and 5% ($> 100 \text{ MeV}$). The present work used a similar distribution, except for the fact that all neutrons with energy larger than 10 MeV were condensed in one energy group with 25% probability. A monodirectional, vertical incidence from the room ceiling was assumed. An event rate of 0.03 evt/kgd was thereby calculated, which corresponds to less than 1% of the total signal.

In Table 10 an uncertainty analysis is presented that includes statistical and non-statistical uncertainties Sections 6.1–6.5. In the analysis, uncertainties of 100% are associated for quantities lacking a reliable uncertainty estimate. The sensitivity coefficients (i.e., the relative contribution of each quantity to the total event rate) are included. Based on these results, the calculated event rate is $6.5 \pm 1.0 \text{ evt/kgd}$ neglecting the tank support.

The largest identified uncertainties are the experimental uncertainty in the concrete radio-assay, the presence of gaps in the water shield (uncertainties Sections 6.3(d) and 6.4, respectively). As no major improvement can be expected in the first item, it is desirable to re-arrange the water shield in order to eliminate the gaps before the execution of the next experiments.

7. Effect of the tank support

The support structure above the tank pedestal was not considered in the present work, leaving the space between the tank and the pedestal to be filled by materials chosen on the basis of future simulations. An idea of the importance of this structure can however be obtained by considering a worst-case situation in which the support is simply a massive 32 cm-thick block of pine wood. Woods in general contain about 50% carbon, 6% hydrogen and 44% oxygen (weight %), with trace amounts of several metal ions [19]. As standard densities of white pine wood range between 0.35 and 0.5 g cm^{-3} , a density of 0.4 g cm^{-3} was used for the simulation. The simulations (considering neutrons from concrete) showed that a wood block alone would attenuate the neutrons by a factor of 6.6, reducing the event rate to 1.0 evt/kgd.

With an additional shielding of 10 cm polyethylene (CH_2 , density 0.95 g cm^{-3}) between the wood and the tank, the event rate is further reduced to 0.2 evt/kgd. These results demonstrate the possibility to achieve event rates smaller than 1 evt/kgd using an additional neutron shielding layer below the tank. Furthermore, the results indicate that the precision of the neutron background estimate for SIMPLE can be strongly improved by including a detailed description of the tank support in the MCNP model.

8. Conclusions

Based on MCNP simulations, a neutron shield was implemented for the SIMPLE experiment that allowed to reduce the event rate to less than 6 evt/kgd. In the present configuration, the dominant contribution to the neutron-induced signal originates from the concrete pedestal that supports the tank in which the SDDs are immersed. Neutrons emitted in the spontaneous fission of ^{238}U and from (α, n) interactions due to the decay of ^{232}Th and ^{238}U in concrete have similar contributions to the detector signal. A rough estimate indicates that neutrons emitted from the cavern surface due to muon interactions with the rock have a negligible contribution to the neutron-induced background.

The model precision is currently limited by non-statistical uncertainties. These include, in first place, the presence of gaps in the water shield and the unaccounted wooden support between the tank and the concrete pedestal. In second place, the measurement of the concrete density and neutron emitters in the shield water are important aspects to clarify.

The results also indicate the potential for a further reduction in the neutron-induced background in the SDDs, namely through the re-arrangement of the water shield eliminating the gaps and using an additional hydrogen-based shield under the tank for protection from the pedestal. These modifications will be implemented in the next phase of the SIMPLE project.

Acknowledgments

The Director, Stephane Gaffet, and staff of LSBB are gratefully acknowledged for their assistance in various stages of the work. We thank Dr. Christophe Emblanch (University of Avignon) for the chemical analysis of the site concrete and rock. Dr. Pia Loaiza (Laboratoire Souterrain de Modane) is acknowledged for the radio-assays of concrete and steel. We also thank Dr. Thomas Girard (University of Lisbon) for his encouragement and assistance in the article writing. This work was supported in part by Grant PDC/FIS/83424/2006 of the Portuguese Foundation for

Science and Technology (FCT), and by the Nuclear Physics Center of the University of Lisbon. The work of Miguel Felizardo is supported by FCT Grant SFRH/BD/46545/2008.

References

- [1] <<http://lsbb.oca.eu/>>, 20 April, 2010.
- [2] T.A. Girard, et al., Phys. Lett. B 621 (2005) 233. doi:10.1016/j.physletb.2005.06.070.
- [3] M. Felizardo, et al., arXiv:astro-ph/1003.2987v1.
- [4] H. Wulandari, J. Jochum, W. Rau, F. von Feilitzsch, arXiv: hep-ex/0401032.
- [5] V.A. Kudryavtsev, for UKDMC, ZEPLIN-II and ILIAS, J. Phys.: Conf. Ser. 120 (2008) 042028. doi:10.1088/1742-6596/120/4/042028.
- [6] A. Lindote, H.M. Araújo, V.A. Kudryavtsev, M. Robinson, Astropart. Phys. 31 (2009) 366. doi:10.1016/j.astropartphys.2009.03.008.
- [7] V.A. Kudryavtsev, L. Pandola, V. Tomasello, Eur. Phys. J. A 36 (2008) 171. doi:10.1140/epja/i2007-10539-6.
- [8] D.-M. Mei, C. Zhang, A. Hime, Nucl. Instr. and Meth. A 606 (2009) 651. doi:10.1016/j.nima.2009.04.032 Data available from <<http://neutronyield.usd.edu/>>, 20 April, 2010..
- [9] X-5 Monte Carlo Team, MCNP-A General Monte Carlo N-Particle Transport Code, Version 5. LA-UR-03-1987, Los Alamos National Laboratory, Los Alamos, NM, 2003.
- [10] J. Amaré, et al., J. Phys.: Conf. Ser. 39 (2006) 151. doi:10.1088/1742-6596/39/1/035.
- [11] H. Wulandari, J. Jochum, W. Rau, F. von Feilitzsch, Astropart. Phys. 22 (2004) 313. doi:10.1016/j.astropartphys.2004.07.005.
- [12] V. Chazal, et al., Astrpart. Phys. 9 (1998) 163.
- [13] J.K. Shultis, R.E. Faw, in: Radiation Shielding, Prentice Hall, Upper Saddle River, NJ, 1996.
- [14] <<http://sws.irsn.fr/sws/mesure/index>>, 20 April, 2010.
- [15] MINURAR: Minas de Urânio e seus resíduos: efeitos sobre a saúde da população -Relatório Científico I, National Health Institute, Lisbon, 2005.
- [16] M. Beyermann, T. Bünger, K. Gehrcke, D. Obrikat, Strahlenexposition durch natürliche Radionuklide im Trinkwasser in der Bundesrepublik Deutschland, Federal Office for Radiation Protection, Saltzgitter 2009. urn:nbn:de:0221-20100319945.
- [17] E.F. Shores, Nucl. Instr. and Meth. B 179 (2001) 78. doi:10.1016/S0168-583X(00)00694-7.
- [18] D.-M. Mei, A. Hime, Phys. Rev. D 73 (2006) 053004. doi:10.1103/PhysRevD.73.053004.
- [19] R.C. Pettersen, in: R.M. Rowell (Ed.), The Chemistry of Solid Wood, American Chemical Society, Washington, DC1984, pp. 57–126.